Int J Thermophys (2009) 30:810–832
DOI 10.1007/s10765-009-0582-6

Turbidity Data of Weightless SF_6 Near its Liquid–Gas Critical Point

C. Lecoutre · Y. Garrabos · E. Georgin · F. Palencia · D. Beysens

Received: 28 July 2007 / Accepted: 31 March 2009 / Published online: 2 May 2009

Abstract Light transmission measurements performed in SF_6 close to its liquid–gas critical point are used to obtain turbidity data in the reduced temperature range $\frac{T-T_c}{T_c} = [1.6 \times 10^{-7} - 1.6 \times 10^{-3}]$ (T is temperature, T_c is the critical temperature). Automatic experiments (ALICE 2 facility) were made at a near critical density, i.e., $\frac{\langle\rho\rangle-\rho_c}{\rho_c} = 0.8\,\%$, in the one-phase homogeneous region, under the microgravity environment of the Mir Space Station ($\langle\rho\rangle$ is the average density, ρ_c is the critical density). The turbidity data analysis verifies the theoretical crossover formulations for the isothermal compressibility κ_T and the correlation length ξ. These latter formulations are also used to analyze very near T_c thermal diffusivity data obtained under microgravity conditions by Wilkinson et al. (Phys. Rev. E **57,** 436, 1998).

Keywords Turbidity · Adiabatic piston effect · SF_6 · Microgravity experiment · Ornstein–Zernike theory

1 Introduction

Close to their liquid–gas critical point, pure fluids behave as three-dimensional (3D) Ising-like systems with universal features predicted for the corresponding {$d = 3$,

C. Lecoutre (✉) · Y. Garrabos · E. Georgin · F. Palencia
ESEME-CNRS, Institut de Chimie de la Matière Condensée de Bordeaux,
UPR 9048, Université Bordeaux I, 87 Avenue du Dr. A. Schweitzer,
33608 Pessac Cedex, France
e-mail: lecoutre@icmcb-bordeaux.cnrs.fr

D. Beysens
ESEME-CEA-ESPCI, PMMH, UMR CNRS 7636, Universités Paris 6 et Paris 7, 10, Rue Vauquelin,
75231 Paris Cedex 05, France

$n = 1\}$ universality class [1,2]. d is the space dimension, while n is the dimension of the order parameter (OP) density. However, the singular universal behavior of the critical fluids makes their experimental study difficult in presence of the effect of gravity which distorts the local density and hinders measurements [3]. It is now well established that experimenting very close to the critical point of pure fluids takes great benefit of a microgravity environment [4]. Sulfur hexafluoride (SF_6) was one among the most convenient working fluids that was used in weightlessness to investigate such critical-point phenomena. Indeed, SF_6 shows a moderate critical pressure p_c ($\simeq$3.8 MPa) and critical temperature T_c ($\simeq$ 45.6 °C) that permit easy experimentation.

In this article, we report light transmission measurements (turbidity data) at constant (near-critical) density that were carried out in a SF_6 sample very close to its critical point under microgravity conditions. These measurements were performed in the ALICE 2 facility [5] on-board the MIR station. In the automatic management of the facility, the light transmission measurements were essential for determining the critical temperature (T_c) and to verify whether the fluid is at thermodynamic equilibrium. This was especially needed in the temperature range $T - T_c < 100$ mK (T is temperature) where density equilibration times can become tremendously long due to the well-known "critical slowing down." Equilibration at temperatures as close as $\sim$100 μK from T_c could be optically checked in the ALICE 2 facility (see below). In this work, turbidity data have then been obtained over more than three temperature decades, in the range $\Delta\tau^* = [1.6 \times 10^{-7} - 1.6 \times 10^{-3}]$. (Here $\Delta\tau^* = \frac{T-T_c}{T_c}$ is the reduced temperature distance to the critical temperature $T_c = 318.733$ K).[1] The analysis of turbidity data in such a temperature range has been made in terms of the Ornstein–Zernike theory [6,7] without any adjustable parameters. In this analysis of the turbidity measurements, the singular and cross-over behaviors of a number of thermodynamic quantities have been verified, in particular the correlation length of density fluctuations, ξ, and the isothermal compressibility, κ_T, using the mean crossover functions for κ_T ($\Delta\tau^*$) and ξ ($\Delta\tau^*$) as recently estimated in Ref. [8].

The article is organized as follows. In Sect. 2, the turbidity measurements are described with special attention to the sample equilibration in a microgravity environment. Section 3 deals with data analysis using the Ornstein–Zernike theory. Section 4 shows the application of the present theoretical support to the description of the thermal diffusivity measurements of Wilkinson et al. [9].

2 Turbity Measurements Using the ALICE 2 Facility

2.1 Turbidity Measurements

A typical turbidity experiment involves measurements of the light intensity ratio $R = I_2/I_1$, where I_1 is the incident light from the entrance optics and I_2 is the transmitted light through the fluid. The turbidity τ_{expt} is related to R by the equation

[1] $T_c = 318.733$ K results from the pVT data of Biswas et al. [26,27] for $\varrho \simeq 734.3$ kg. m^{-3}; this value is also consistent with pVT data from Refs. [24] and [28].

$$\tau_{\text{expt}} = \frac{\ln(R)}{e} + B_\tau \tag{1}$$

where e is the sample thickness and B_τ is an adjustable constant that accounts for components in the optical path and intensity normalization of the photodiode response. The automatic measurements of I_1, I_2, and R were performed using the ALICE 2 facility [5] in the weightlessness environment of the MIR Space Station during the Cassiopea French–Russian mission (August 1996).

The ALICE 2 instrument was an advanced optical, thermal, and mechanical facility operating a thermostat of very accurate thermal regulation, allowing 10 µK of relative temperature accuracy and 40 µK · h^{-1} of temporal stability, in the range of 30 °C to 60 °C. Two optical cells labeled IOC and DOC were housed in the thermostat and observed through a Twyman–Green interferometer and by transmission, respectively, as shown in Fig. 1. The DOC could also be used to record the light scattered at small angles and for microscopic observations. Only the DOC cell was used for laser light intensity measurements providing the turbidity data of present interest. Here it is essential to note that this same cell was previously used in the BEM3 experiment performed in the Critical Point Facility (CPF) during the IML 2 mission (July 1994) [10]. This explains our particular attention to provide complete understanding of the fluid behavior in such a cell design for a long time period of management in the different

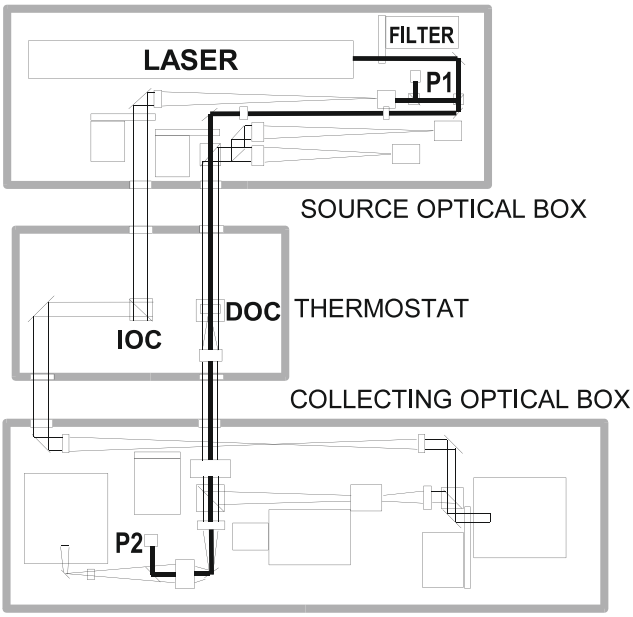

Fig. 1 Enhanced partial scheme of the ALICE 2 optical system activated in intensity measurements of the incident laser light using the photodiode P1 (located in the source optical box) and transmitted laser light through the sample cell (labeled DOC) located in the thermostat, using the photodiode P2 (located in the collecting optical box). The complete optical scheme is detailed in [5]

environments needed by the space missions. The fluid under study is SF_6 of electronic quality, corresponding to 99.98 % purity (from Alpha Gaz–Air Liquide). The sample cell volume was a highly symmetrical and cylindrical cell of $D = 12$ mm inner diameter and $e = 3.023$ mm inner thickness, providing a fixed fluid volume $V \sim 150\,\mathrm{mm}^3$. This cell, whose thermal response can be estimated using a pancake cell model [11], was filled in March 1993 at a mean density $\langle\rho\rangle$ slightly greater than the critical density ρ_c, in accordance with our scientific requirements of the phase separation study (not reported here). The relative density deviation $\langle\delta\rho^*\rangle = \frac{\langle\rho\rangle-\rho_c}{\rho_c} = (0.8 \pm 0.1)\,\%$ was estimated on earth using a precise optical method [12] based on the relative variation of the position of the liquid–gas meniscus, as a function of $T - T_c$. We recall that this determination of the off-critical density deviation does not need the critical density to be known.

All the microgravity experiments were systematically started by the determination of the transition temperature T_{coex} to compare with the T_c value previously estimated on Earth with a relative precision of ± 0.5 mK, larger than the expected $T_c - T_{coex} \sim 30\,\mu$K difference (here $T_{coex} \neq T_c$ since $\langle\rho\rangle \neq \rho_c$, see below). The fluid was initially heated at 0.5 K above T_c and then stabilized for 1 h in order to obtain an equilibrium fluid state. After this cell homogenization, the determination of T_{coex} used an automatic procedure based on successive negative temperature steps to observe the phase separation. Each automatic step was made of temperature quenches of amplitude δT_n (selected from 100 mK to 0.3 mK) performed closer and closer to T_{coex} and followed by a waiting time of duration δt_w (selected from 600 s to 1800 s). An automatic temperature quench from $T - T_c + \delta T_n$ to $T - T_c > 0$ (i.e., a quench performed in the homogeneous domain) produced a continuous transient decrease of the transmitted light. The transition temperature T_{coex} was then detected by an abrupt transient change in the transmitted light during the T_{coex} crossing quench from $T - T_c + \delta T_n > T_{coex}$ to $T - T_c < T_{coex}$. The automatic procedure was repeated with smaller and smaller δT_n values until the determination of T_{coex} was returned with a stabilized mK digit. The results reported here are concerned by the three temperature steps $\delta T_n\,(\mathrm{mK}) = \{3;\ 1;\ 0.3\}$ with $\delta t_w = 1200$ s (see Fig. 2), which allowed T_{coex} to be found at the same value as determined on Earth, within the expected (± 0.5 mK) resolution.

After that automatic procedure and a new cell homogenization at $T_{coex} + 0.5\,K$, the refined value of T_{coex} was obtained using a programmed sequence of temperature quenches leading to the direct observation of the phase transition phenomena. The final part of this sequence used a series of the smallest temperature step $\delta T_{10} = 100\,\mu$K allowed by the ALICE 2 facility, with raising the waiting period up to $\delta t_w = 2460$ s. Indeed, the post-flight analysis of the phase separation process allowed the determination of T_{coex} with a resolution lower than 50 μK (see below). The turbidity data analyzed here are then obtained from seven (automatic and/or programmed) sequences performed during a complete experiment of 69.5 h (i.e., a 3-day experiment dedicated to the phase separation study). For the seven runs, the measurement of T_{coex} was reproduced within 15 μK (with 1 μK temperature resolution), thanks to the high thermal stability (± 3 μK) of the YSI 44908 thermistors used for the temperature regulation system. As a result, T_{coex} was then estimated to be 45.557270 °C (± 15 μK). However, in spite of its low power value (≤ 100 μW close to T_{coex}) [5], a weak part ($\sim 2 \times 10^{-6}$) of the beam power is absorbed in the sapphire windows, then inducing a local weak

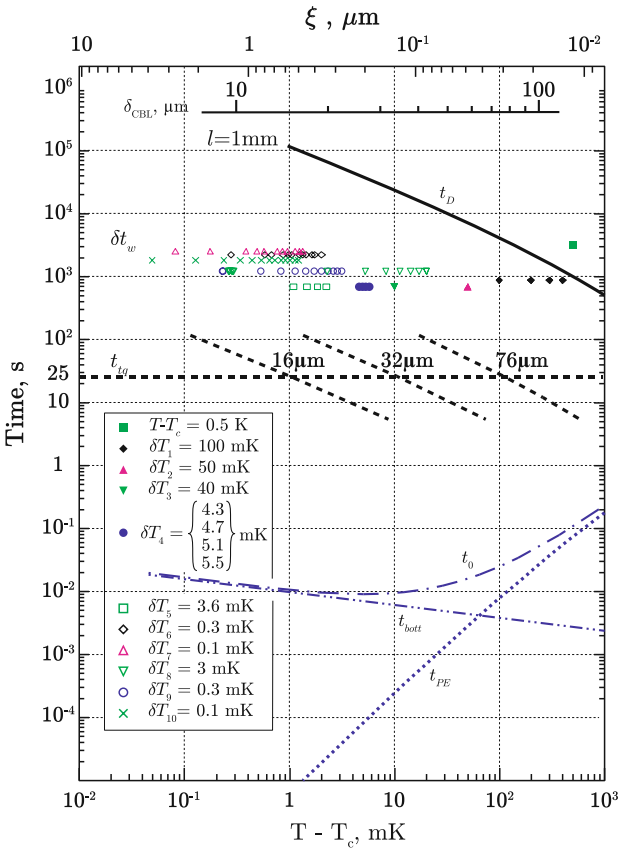

Fig. 2 Characteristic times t_D, t_{PE}, t_{bott}, t_0, δt_w, t_{tq}, (expressed in s), as a function of the temperature distance $T - T_c$ (expressed in mK); t_D of Eq. 2: (slow) thermal diffusivity (*full black curve* labeled t_D); t_{PE} of Eq. 3: (fast) adiabatic piston effect in the ideal conductivity regime (*dotted blue curve* labeled t_{PE}); t_{bott} of Eq. 4: adiabatic piston effect in the conductivity bottleneck regime (*double dotted dashed blue curve* labeled t_{bott}) and t_0 of Eq. 5: effective adiabatic piston effect (*mixed blue curve* labeled t_0). The length scale of the direct observation cell is $l = 1$ mm; δt_w (colored symbols): waiting time period after each temperature quench of amplitude δT_n (see inserted table) and time duration $t_{tq} = 25$ s (see horizontal tireted line). Three dashed curves: typical diffusive relaxation time of Eq. 2 over the typical thickness $\delta_{CBL} = 76\,\mu$m, 32 μm, and 16 μm (see label) of the cold boundary layer at the end ($t = t_{tq} = 25$ s) of a temperature quench at $T - T_c = 100$ mK, 10 mK, and 1 mK, respectively (see text for detail). First upper axis: thermal penetration length $\delta_{CBL}\left(t_{tq} = 25\,\text{s}\right)$ (expressed in μm) of cold boundary layer during $t_{tq} = 25$ s. Second upper axis: correlation length ξ (expressed in μm) of fluctuating density

temperature gradient in the fluid [13], which can affect the above determination of the transition temperature. A more realistic uncertainty on the value was then estimated as $\pm\frac{\delta T_{10}}{2} = \pm 50\,\mu$K. Note that the absolute calibration of the temperature sensors of the thermostat was not made as this level of resolution. Therefore, T_{coex} is a value associated with the "thermal insert" setup (including the DOC cell) operated by the

ALICE 2 facility.[2] Considering the deviation $\langle \delta\rho^* \rangle = +0.8\,(\pm 0.1)\,\%$ to the selected critical density (see below), the relative temperature distance $T_c - T_{coex}$ can be estimated to 27 (± 4) μK[3] and then all the temperature distances reported hereafter are measured from $T_c(\text{cell}) = 45.557297\,^\circ\text{C}$ (we recall that our selected literature value is $T_c\,(SF_6) = 45.583\,^\circ\text{C}$, see Footnote 1). We underline here the high reliability (no leak, no impurity) of this optical cell. Indeed, this cell, initially filled with SF_6 three years before this Cassiopea mission, had already been used during the IML2 mission (1994), and was re-used in the MIR station until 2000, showing a reproducibility of the transition temperature value at 1 mK level. The turbidity data analyzed here cover the temperature range from 50 μK to 500 mK above T_c, i.e., $1.5 \times 10^{-7} \leq \Delta\tau^* \leq 1.5 \times 10^{-3}$. We will discuss later in this article the influence of the relative critical density difference (hence the relative critical temperature difference), on turbidity measurements.

The light intensity measurements used the ALICE 2 optical setup underlined in Fig. 1. A He–Ne laser provided a $\lambda_0 = 632.8$ nm (red) monochromatic light with about 1 mW maximum power (λ_0 is the incident laser light wavelength in vacuum). Laser stability after 1 h was estimated to be better than 0.3 %. The intensity I of the laser beam was measured by means of two photodiodes before (I_1) and after (I_2) having passed through the fluid cell. A total of 1 % of the laser intensity was directed toward the photodiode P1 of the source optical box, and 93 % in a 0.32 mm diameter parallel beam directed through the fluid cell. In the collection optical box, the central part of the beam was reflected by a mirror to a photodiode P2 identical to the photodiode P1. A filtering hole was placed just before P2 in order to reduce multiple scattering. This system was giving 0.3 % precision on measurements covering a relative amplitude range of 500, thanks to two magnification values (of ratio 10.3), selected by a relay placed on the current amplifier. For each experiment, the ALICE 2 Data Handling System (DHS) recorded a complete set of scientific and technical data at a 25 Hz sampling rate. Here we are concerned by the sample cell temperature, the incident and transmitted light intensities and their corresponding ratio, which were jointly analyzed with each synchronized video picture of the cell observed in wide-field transmission.

2.2 Experimental Control of the Sample Equilibration Related to the Piston Effect

When approaching the liquid–gas transition along the critical isochore in the homogeneous domain ($T > T_c$), the time duration δt_w of the waiting period after each temperature step δT_n, was programmed taking into account the characteristic times for temperature equilibrium and density equilibrium, respectively. As a matter of fact, it is now well established that the temperature equilibrium of the fluid sample is first related to the fast adiabatic piston effect [14] of characteristic time t_{PE}. Density equilibrium

[2] The "ALICE 2" value of the transition temperature, $T_{coex}(SF_6/\text{ALICE 2}) = 45.557270\,^\circ\text{C}$, well compares with the "CPF" one, $T_{coex}(SF_6/\text{CPF}) = 45.532500\,^\circ\text{C}$, which was found during the IML2 mission (1994) using an analogous thermal setup made of the same fluid sample located inside another similar thermostat monitored by the Critical Point Facility (CPF).

[3] The temperature difference $T_c - T_{coex}$ was estimated for $\Delta\rho^*_{LV} = \langle \delta\rho^* \rangle$, using the power law $\Delta\rho^*_{LV} = B\left(\Delta\tau^*\right)^\beta$ where $\Delta\rho^*_{LV} = \frac{\rho_L - \rho_V}{2\rho_c}$, $B = 1.596$, and $\beta = 0.32575$ (ρ_L and ρ_V are the coexisting liquid and vapor densities, respectively).

then slowly follows by diffusive transfer from the boundary layers [9], with the thermal diffusion characteristic time t_D. The singular behaviors of t_{PE} and t_D approaching T_c were estimated considering the following approximated expressions (using standard notations):

$$t_D = \frac{l^2}{D_T} \propto \left(\Delta\tau^*\right)^{-\gamma+x_\lambda} \tag{2}$$

and

$$t_{PE} = \frac{t_D}{(\gamma_0 - 1)^2} \propto \left(\Delta\tau^*\right)^{\gamma+x_\lambda-2\alpha} \tag{3}$$

when $\Delta\tau^* \to 0$. In Eq. 2, $l = \frac{V_{fluid}}{A_{CBL}}$ [14–16] is the characteristic length of an "ideal" experimental cell made of materials of infinite conductivity [V_{fluid} is the cell volume, A_{CBL} is the external cell area where the cold boundary layer (CBL) develops during the quench]. The actual sample geometry leads to $l \approx 1$ mm. D_T is the thermal-diffusivity coefficient and $\gamma_0 = \frac{c_p}{c_V}$ is the ratio between the specific heat at constant pressure and the specific heat at constant volume. The asymptotic power laws of Eqs. 2 and 3 need to recall the main results (using standard notations) of the mode coupling theory of transport properties and renormalization group approach of critical dynamics:

- $D_T = \frac{\lambda}{\rho c_p} \sim \frac{1}{\eta_S \xi} \propto (\Delta\tau^*)^{\gamma-z_\lambda}$ where $c_p \sim \kappa_T \sim \chi \propto \xi^{2-\eta} \propto (\Delta\tau^*)^{-\gamma}$ is the specific heat at constant pressure, κ_T is the isothermal compressibility, χ is the susceptibility, and $\xi \propto (\Delta\tau^*)^{-\nu}$ is the correlation length. The critical exponent $\gamma = \nu(2-\eta) = 1.2396$ is here expressed in terms of the two critical exponents $\nu = 0.6304$ and $\eta = 0.0336$ [17] of the correlations functions of the size and decay rate of the order parameter fluctuations;
- $c_V \propto (\Delta\tau^*)^{-\alpha}$ [with $\alpha = 2 - d\nu \simeq 0.11$ [17] for $d = 3$], leading to the practical power law: $\gamma_0 \simeq \gamma_0^+ (\Delta\tau^*)^{-(\gamma-\alpha)}$ (with $\gamma - \alpha \simeq 1.13$);
- $\lambda = \left(\lambda^c + \lambda^b\right) \propto (\Delta\tau^*)^{-x_\lambda}$ is the total thermal conductivity written as a sum of a background term λ^b and a critical term $\lambda^c \propto \xi^{z_\lambda} \propto (\Delta\tau^*)^{-x_\lambda}$ (with $z_\lambda = \frac{x_\lambda}{\nu} \simeq 0.89808$, i.e., $x_\lambda \simeq 0.56615$);
- $\eta_S = \eta_0 (Q_0\xi)^{z_\eta} \propto (\Delta\tau^*)^{-x_\eta}$ is the shear viscosity written as a multiplicative anomaly between a regular term $\eta^b = \eta_0$ and a critical term $\eta^c \propto \xi^{z_\eta}$ [with $z_\eta \simeq 0.06832$, [18][4] (i.e., $x_\eta = \nu z_\eta \simeq 0.0430$), and the scaling law $\gamma - x_\lambda = \nu\left(1 + z_\eta\right)$ or $z_\lambda + z_\eta = \varepsilon - \eta$, with $\varepsilon = 4 - d$].

As a result, for $\Delta\tau^* \to 0$, t_D goes to infinity with the critical exponent $-\gamma + x_\lambda \simeq -0.67$ while t_{PE} goes to zero with the critical exponent $\gamma + x_\lambda - 2\alpha \simeq 1.59$. At the Cassiopea mission time, from the available expressions for D_T, κ_T, c_V [19–21], and c_p, using $c_p - c_V = \frac{T}{\rho}\left(\frac{\partial p}{\partial T}\right)_\rho^2 \kappa_T$ (with $\gamma_c' = \left(\frac{\partial p}{\partial T}\right)_{\rho_c} = 0.0835\,\text{MPa}\cdot\text{K}^{-1}$, see below), we obtained $\gamma_0^+ \approx 7.0\,10^{-2}$. In Fig. 2, the estimated singular behaviors of t_D

[4] The value of $z_\eta = 0.06832$ is calculated from Eq. (6.4) of this reference, with $J_1 = \frac{1}{15}\left(1 - \frac{\eta}{2}\right)^2$ and $\eta = 0.0336$ (see Ref. [17]).

and t_{PE} with $l = 1$ mm are represented as a function of $T - T_c$ by the full black curve (labeled t_D) and the dotted blue curve (labeled t_{PE}), respectively. Upon approaching the critical point, the two curves illustrate the increasing contrast between the fast acceleration of the temperature equilibration by the piston effect mechanism and the critical slowing down of the diffusive process of density equilibration.

However, in the closest temperature range $0.3\,\text{mK} \lesssim T - T_c \lesssim 5\,\text{mK}$, the conductivity bottleneck effect [22,11] is dominant, due to the thermal impedance ratio $\frac{Z}{Z_i} \ll 1$ [11]. $Z = (\lambda \rho_c c_P)^{-\frac{1}{2}}$ is the thermal impedance of the fluid while $Z_i = \left(\lambda_i \rho_i c_{P,i}\right)^{-\frac{1}{2}}$ is the thermal impedance of the cell material labeled with the subscript i. We can use the simplified pancake cell model [11] to calculate the effective thermal impedance Z_{cell} of our high symetrical experimental cell of aspect ratio $\frac{e}{D} \simeq \frac{1}{4}$. The spacer ($i = S$) is here made of copper-cobalt-beryllium alloy and the windows ($i = W$) are made of sapphire. As a result, the cell thermal impedance $Z_{cell} = \frac{Z_S Z_W (1+2\frac{e}{D})}{Z_S + 2\frac{e}{D} Z_W} \simeq 5.1 \times 10^{-5}\,\text{m}^2 \cdot \text{K}^2 \cdot \text{W}^{-1} \cdot \text{s}^{-\frac{1}{2}}$ is well larger than Z of the fluid for $T - T_c \lesssim 5\,\text{mK}$ [11] and the temperature equilibration of the fluid is also a material-dependent quantity. Accounting then for the asymptotical condition $\gamma_0 = \frac{c_P}{c_V} \gg 1$, the new singular behavior of the characteristic time t_{bott} in the bottleneck regime can be written as

$$t_{bott} = (\ell Z_{cell} \rho c_V)^2 \propto \left(\Delta\tau^*\right)^{-2\alpha} \tag{4}$$

From the comparison of the two limiting Eqs. 3 and 4, the critical decrease of t_{PE} levels off in the conductivity bottleneck regime close to the critical point where t_{bott} should rise as c_V^2 (see the blue curve labeled t_{bott} in Fig. 2). Obviously, the complete analysis accounts for the respective surface areas A_S and A_W of each material involved in the heat exchange, leading to define the characteristic time of the temperature equilibration as

$$t_0 = \frac{\ell_{eff}}{D_T} \frac{1}{(\gamma_0 - 1)^2} \tag{5}$$

where the new effective characteristic length of our pancake cell is given by $\ell_{eff} = \frac{\ell}{Z}\left(\frac{A Z_S Z_W}{Z_S A_W + Z_W A_S}\right)$. Equation 5 resumes to the two limiting regimes of Eq. 3, valid for $Z_i \ll Z$ far from T_c, and Eq. 4, valid for $Z_i \gg Z$ close to T_c (as shown by the curve labeled t_0 in Fig. 2).

Figure 2 shows that the characteristic time t_0 of the temperature equilibration remains lower than 20 ms in the temperature range $T - T_c \lesssim 100\,\text{mK}$. On the other hand, a careful analysis of the SCU temperature variation shows that any thermal quench was performed in about 5 s to 8 s, while the residual small temperature oscillations are damped after ~25 s. We have then taken t_{tq}~25 s as a typical time duration of a non-zero value of the (removed) heat flux at the cell wall-fluid boundary. During t_{tq}, the piston effect was very efficient to thermalize the bulk fluid, especially in the temperature range of the bottleneck regime [22,11] where its characteristic time t_0 is at least three order of magnitude lower than t_{tq} (see Fig. 2). Therefore, accounting in advance only for the diffusive density relaxation process has provided the main time-line con-

straint in order to plan the automatic cell management and data storage of the Cassiopea mission. In Fig. 2 for example, for each final fluid state at $T - T_c$, we have reported the δt_w, $T - T_c$ points (see the different colored symbols). The δt_w values range from 800 s to 2400 s. The waiting period was then optimized considering the density relaxation of the cold boundary layer which has developed during each temperature quench. Indeed, the typical values of the thermal penetration length $\delta_{CBL} \simeq \left(D_T t_{tq}\right)^{\frac{1}{2}} \ll l$ of the cold boundary layer are $\delta_{CBL} \simeq 76\,\mu m$ at $T - T_c \simeq 100\,mK$, $\delta_{CBL} \simeq 32\,\mu m$ at $T - T_c \simeq 10\,mK$, and then such that $\delta_{CBL} \lesssim 16\,\mu m$ for $T - T_c \lesssim 1\,mK$. This critical decrease, as $\delta_{CBL} \propto (\Delta\tau^*)^{\frac{\gamma - x_\lambda}{2}}$ with $\frac{\gamma - x_\lambda}{2} \simeq 0.335$, is illustrated in the upper horizontal axis labeled δ_{CBL} of Fig. 2. For comparison, a second upper axis also shows the critical increase of the size ξ of the density fluctuations approaching the critical temperature (with $\xi \lesssim \lambda_0$ in the temperature range $T - T_c \gtrsim 0.1\,mK$). Due to the adiabatic piston effect during the thermal quench period $0 \lesssim t \lesssim t_{tq}$, the homogeneous bulk density was decreased and became closer to the true critical density since the off-critical filling density of the cell was positive. Correlatively, the mean density within the cold boundary layer was increased. During the subsequent waiting period $t_{tq} \lesssim t \lesssim \delta t_w$, the bulk density relaxed toward the off-critical density, while the density gradients within the boundary layer were decreasing. The waiting time was then selected to reduce the density gradients by a factor $\sim \left(\frac{\delta t_w}{t_{tq}}\right)^{\frac{1}{2}}$, due to the diffusive penetration of the cold boundary layer. Therefore, the slight increase of δt_w for $(T - T_c) \to 0$, follows as well as possible the diffusive critical slowing down at the CBL length scale. This result was illustrated in Fig. 2 by three curves of Eq. 2 labeled by the thickness (76 µm, 32 µm, and 16 µm) of the cold boundary layer after (i.e., at $t = t_{tq} \simeq 25$ s) the transient duration of a thermal quench performed at $T - T_c \simeq 100\,mK$, 10 mK, and 1 mK, respectively. Using the waiting period given in Fig. 2, the density gradients were then reduced by a factor ranging from 5.6 to 10.

In addition, in the temperature range $T - T_c \geq 1\,mK$ we have assumed that any local temperature deviation δT_x at the point x, after the quenching time scale $t_{tq} \gg t_{PE}$, was lower than 10 % of a quench depth $|\delta T_n| = 0.1(T - T_c)$, leading to $\delta T_x \leq 0.01(T - T_c)$. Then, the relative density deviation $\frac{\delta\rho_b}{\langle\rho\rangle}$ in the homogeneous bulk was given by $\frac{\delta\rho_b}{\langle\rho\rangle} \lesssim -0.01\Delta\tau^* T_c \alpha_S$ [where $\alpha_S = -\frac{1}{\rho}\left(\frac{\partial\rho}{\partial T}\right)_S \propto (\Delta\tau^*)^{-\alpha}$ is the isentropic thermal expansion coefficient (expressed in K^{-1})]. From $\frac{c_V}{\alpha_S} = -\frac{T}{\rho}\left(\frac{\partial p}{\partial T}\right)_\rho$, we have obtained

$$\frac{\delta\rho_b}{\langle\rho\rangle} \lesssim \frac{-0.01\Delta\tau^* c_V^*}{(Y_c + 1)(1 + \Delta\tau^*)} \simeq -0.041\Delta\tau^* \frac{(\Delta\tau^*)^{-\alpha} + 0.651}{1 + \Delta\tau^*}$$

In the above equation, we have used $c_V^* = \frac{m_{\tilde{P}}}{k_B} c_V = Z_c \frac{\rho_c T_c}{p_c} c_V = \frac{A^+}{\alpha}(\Delta\tau^*)^{-\alpha} + B_{C_V}$ with $A^+ = 0.875$, $\alpha = 0.1075$, and B_{C_V}=5.3 [20,21], at $\langle\rho\rangle \cong \rho_c$. Similarly, within the conductive cold boundary layer, $\frac{\langle\delta\rho_{CBL}\rangle}{\langle\rho\rangle} \lesssim -0.01\Delta\tau^* T_c \alpha_p$ [where $\alpha_p = -\frac{1}{\rho}\left(\frac{\partial\rho}{\partial T}\right)_p$ is the isobaric thermal expansion coefficient (expressed in K^{-1})].

From $\alpha_p = \kappa_T \left(\frac{\partial p}{\partial T}\right)_\rho = \alpha_S \left(1 - \frac{c_p}{c_v}\right) \simeq -\alpha_S \gamma_0 \simeq -\alpha_S \gamma_0^+ (\Delta\tau^*)^{-(\gamma-\alpha)}$, we have obtained

$$\frac{\langle \delta\rho_{CBL} \rangle}{\langle \rho \rangle} \lesssim \frac{0.01\,(\Delta\tau^*)^{1-\gamma+\alpha}\,\gamma_0^+ c_V^*}{(Y_c+1)\,(1+\Delta\tau^*)} \propto 0.00287\,(\Delta\tau^*)^{1-\gamma+\alpha}\,\frac{(\Delta\tau^*)^{-\alpha}+0.651}{1+\Delta\tau^*}$$

at $\langle \rho \rangle \cong \rho_c$. From the above singular behaviors, it is easy to infer that the waiting period of $\delta t_w = 2460$ s after each smallest quench depth $|\delta T_{10}| = 100\,\mu$K was appropriate to reduce the density inhomogeneities within $\pm 0.3\,\%$ at $T - T_c \simeq 1$ mK. In the temperature range $T - T_c < 1$ mK, the quench depth of $|\delta T_{10}| = 100\,\mu$K increases the relative importance of the local temperature deviations, especially in the cold boundary layer. However, the closer to T_c, the smaller the thickness of the boundary layer, hence the fluid volume where the density inhomogeneities occurs (For $T - T_c \lesssim 0.5$ mK, the typical volume of the cold boundary layer at $t = t_{tq} \simeq 25$ s is lower than 1 % of the total fluid volume). Practically, in the temperature range $T - T_c \lesssim 1 - 2$ mK where the smallest quench depth was used, the temperature at any point of the fluid volume follows quasi-instantaneously the wall temperature in the bottleneck regime [22,11]. Especially comparing with the c_V experiments of Straub et al. [20,21], we note that our mean *"fastest"* quench cooling rate $\frac{dT}{dt} \simeq \frac{-\delta T_{10}}{t_{tq}} = -14.4\,\text{mK}\cdot\text{h}^{-1}$ that was used in the T_{coex}-crossing range, is four time smaller than the slowest cooling run of $\frac{dT_0}{dt} = -60\,\text{mK}\cdot\text{h}^{-1}$ for the blind scanning radiation calorimeter at the critical point under microgravity conditions. In the latter case, the authors note that the temperature and density gradients were greatly reduced by the isentropic effect, while the c_V data are distorted by the ramp rate effect only for $T - T_c \lesssim 1$ mK. Then in our optical experiment, in the temperature range $T - T_c \lesssim 2 - 3$ mK, the evolution and the spatial uniformity of the grey level intensity of the full-field images of the sample are of great help (as mentioned above) to control the homogenization of the critical fluid layer during the transient period ($0 < t \lesssim t_{tq}$) of the temperature quench and during the subsequent waiting period ($t_{tq} \lesssim t \lesssim \delta t_w$). Finally, we note that the waiting periods of order of 2400 s after a temperature change of the order of 100 µK close to T_c still remain a good compromise for a few days space experiment in critical fluid samples of millimetric thickness.

2.3 Experimental Results

Light transmission measurements were made at the end of each waiting time period, assuming then that the fluid state has reached thermodynamic equilibrium. The related turbidity data τ_{expt} of Eq. 1 are plotted in Fig. 3 as a function of $T - T_c$ in a log–lin scale, with $B_\tau = (2.04 \pm 0.03)\,\text{cm}^{-1}$. The inserted log–log scale part of Fig. 3 shows the saturation effect due to the singular behavior of the correlation length that increases the light scattering (the so-called fluid opalescence) close to the critical point. In Eq. 1, the thickness e of the cell was carefully measured with a precision of 5 µm $\left(\frac{\delta e}{e} = 0.16\,\%\right)$. The background turbidity B_τ, depending on the ALICE 2 instrumentation, was assumed to be constant in the temperature range $T - T_c \leq 500$ mK. Using

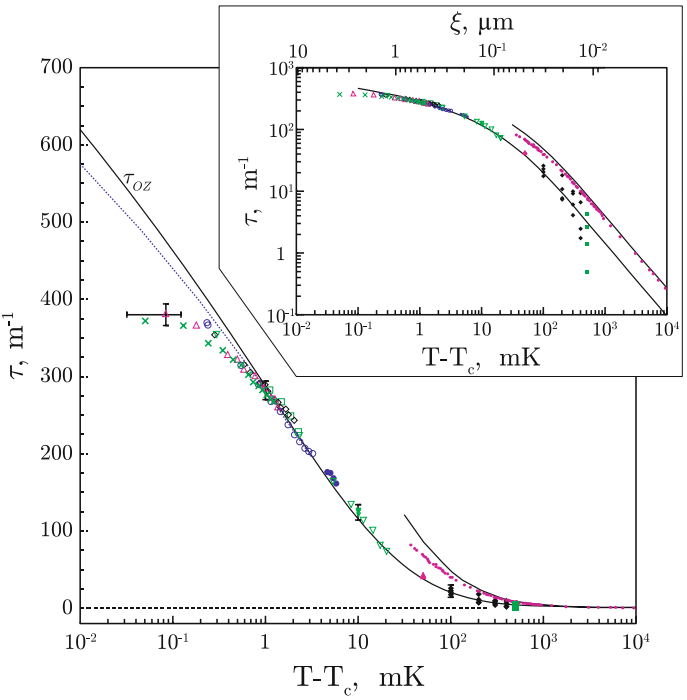

Fig. 3 Lin–log plot of turbidity τ (expressed in m^{-1}) as a function of $T - T_c$ (expressed in mK) obtained from light transmission measurements in SF_6 and compared to Eq. 8 with $\lambda_0 = 632.8$ nm (*left solid curve*) [see Fig. 2 for detail of colored symbols]. Dotted curve represents a correction to Eq. 8 considering the influence close to T_c of the exponent $\eta = 0.0336$ [see Eq. 16]. The horizontal error bar indicates the uncertainty of $\pm 50\,\mu$K on T_{coex}. The vertical error bars come from experimental uncertainty. Other turbidity data from Ref. [23] (*pink disk symbol*) are shown together with the corresponding formulation of Eq. 8, with $\lambda_0 = 466$ nm. Insert is the same in a log–log plot

the raw turbidity measured at $T - T_c \simeq 500$ mK, B_τ has the same mean value as in Earth's calibration of the turbidity offset, with an uncertainty of the order of 1.5 %. For each stabilized final temperature, the measurements of the ratio R results from a 25 Hz data sampling, averaged on at least 1 s. The uncertainty on the R value is around 1 %, leading to an error of ~ 3 % on the measured turbidity, mainly due to the uncertainty in the background turbidity. We recall that the precision level results from scientific requirements of the ALICE 2 facility accounting for "thin" optical cells of millimetric thickness and for a "restricted" dynamic range of 500, with a 0.1 % uncertainty in the calibrated linear response of the photodiodes used for light intensity measurements. However, very close to T_c (i.e., $T - T_c \lesssim 1 - 3$ mK, typically), the error in reduced temperature increases the turbidity error. At $T - T_c \simeq 0.250$ mK for example, we can evaluate the uncertainty on τ_{expt} data to 8 % from the data reproducibility shown in Fig. 3.

3 Turbidity Data Analysis According to Ornstein–Zernike Theory

3.1 Ornstein–Zernike Theory of Light Scattering

Turbidity of a fluid close to its liquid–gas critical point is most essentially due to Rayleigh light scattering by density fluctuations. The scattered light intensity can be written [23] according to Ornstein–Zernike (OZ) [6,7] as

$$I(q) = \frac{AT\kappa_T \sin^2 \Phi}{1 + (q\xi)^2} \tag{6}$$

where q represents the amplitude in the fluid of the transfer wave vector between the incident and scattered light wave vectors: $q = \frac{4\pi n}{\lambda_0} \sin \frac{\theta}{2}$. n is the refractive index of the fluid, and θ is the scattering angle. Φ is the angle between the polarization wave vector of the incident beam and the scattering wave vector. κ_T is the isothermal compressibility and ξ is the long-range fluctuation correlation length. The prefactor A is given by the equation,

$$A = \frac{\pi^2}{\lambda_0^4} \left(\rho \frac{\partial (n^2)}{\partial \rho} \right)_{\mathrm{T}}^2 k_{\mathrm{B}} = \frac{\pi^2}{\lambda_0^4} \left[\frac{(n^2 - 1)(n^2 + 2)}{3} \right]^2 k_{\mathrm{B}} \tag{7}$$

which accounts for geometrical factors, light–fluid scattering cross section, laser optical wavelength λ_0 in vacuum, and Boltzmann constant k_{B}. Turbidity corresponds to the integral of Eq. 6 over all the scattering angles, and one writes according to Puglielli and Ford [23]:

$$\tau_{\mathrm{OZ}} = \pi A T_{\mathrm{c}} \left(1 + \Delta\tau^*\right) \kappa_T F(a), \tag{8}$$

where $F(a)$ is given by the following equation

$$F(a) = \left(\frac{2a^2 + 2a + 1}{a^3} \right) \ln(1 + 2a) - 2 \left(\frac{1 + a}{a^2} \right) \tag{9}$$

with $a = 2\,(k_0 \xi)^2$ and $k_0 = \frac{2\pi n}{\lambda_0}$ (k_0 is the amplitude of the incident light wave vector). The determinations of the physical quantities involved in Eqs. 7–9 are given in the following Sects. 3.2–3.4, while the comparison between τ_{OZ} of Eq. 8 and τ_{expt} of Eq. 1 will be made in Sect. 3.5 and their relative deviation discussed in Sect. 3.6.

3.2 SF_6 Critical Parameters

The 1977 review paper of Watanabe et al. [24] and a survey of more recent literature still shows large discrepancies for the values of the critical point parameters T_{c}, p_{c}, and ρ_{c} of SF_6 (in spite of the high precision level attached to each parameter). The dispersion reflects unexplained large differences (of the order of 8 kPa) on the saturation pressure measurements and the increasing uncertainty (of the order of

Table 1 Critical parameters $\left(\frac{p}{T}\right)_{\mathrm{CP}}$, $\pi_{\rho=\rho_c}$ [see Eq. 10], and $\gamma_c{}' = \left[\left(\frac{\partial p}{\partial T}\right)_{\rho=\rho_c} = \frac{dp_{\mathrm{sat}}}{dT}\right]_{T\to T_c^{\pm}}$ for SF_6

Author	Ref.	$\left(\frac{p}{T}\right)_{\mathrm{CP}} = \frac{p_c}{T_c}$ $\left(\mathrm{MPa}\cdot\mathrm{K}^{-1}\right)$	$\pi_{\rho=\rho_c}$ $\left(\mathrm{kPa}\cdot\mathrm{K}^{-2}\right)$	$\gamma_c{}'$ $\left(\mathrm{MPa}\cdot\mathrm{K}^{-1}\right)$
Biswas et al. ($T > T_c$)	[26]	0.0117778 ($\pm$0.0000035)	0.225 ($\pm$0.005)	0.0835 $\left(^{+0.83\,\%}_{-1.20\,\%}\right)$
Biswas and Ten Seldam	[27]			0.0825285
Watanabe et al.	[24]	0.011795	0.22723	0.0842121
Wagner et al.	[28]	0.0117796		
Funke et al.	[29]	0.0117814	0.226427	0.0839489
Wyczalkowska and Sengers	[30]	0.01178004	0.224143	0.0832181

$\pm 1\,\%$) in the critical density determination when approaching the critical point. The problem was already noted by de Reuck et al. [25] from a critical analysis of the available pVT data from Refs. [24,26–28].

Our selected Biswas et al. value $T_c = 318.733\,\mathrm{K}$ (see above and Footnote 1) agrees with the recommended values $T_c = 318.729\,\mathrm{K}$ by Wagner et al. [28] and $T_c = 318.717\,\mathrm{K}$ by Funke et al. [29]. The values of the critical pressure p_c and the common limiting slope $\gamma_c{}' = \left[\left(\frac{\partial p}{\partial T}\right)_{\rho=\rho_c} = \frac{dp_{\mathrm{sat}}}{dT}\right]_{T\to T_c^{\pm}}$ of the critical isochore ($T \to T_c^{+}$) and the saturation pressure $p_{\mathrm{sat}}(T)$ curve ($T \to T_c^{-}$) are correlated in the $\frac{p}{T}; T$ diagram. They were obtained by fitting the pVT data of Biswas et al. [26,27] with the following asymptotic (linearized) equation

$$\left(\frac{p}{T}\right)_{\rho=\rho_c} = \left(\frac{p}{T}\right)_{\mathrm{CP}} + \pi_{\rho=\rho_c}(T - T_c) \tag{10}$$

with the values of $\left(\frac{p}{T}\right)_{\mathrm{CP}} = \frac{p_c}{T_c}$ and $\pi_{\rho=\rho_c}$ given in Table 1. As shown by the literature data reported in Table 1, our value of $\left(\frac{p}{T}\right)_{\mathrm{CP}}$ agrees with the ones of Wagner et al. [28], Funke et al. [29], and Wyczalkowska and Sengers [30], but differs significantly from the Watanabe et al. value [24], due to their $\sim$8 kPa difference on the saturation pressure measurements. On the other hand, our $\pi_{\rho=\rho_c}$ value is in excellent agreement with the estimated values from the respective fitting equations of the saturation pressure curve of Watanabe et al. [24], Funke et al. [29], and Wyczalkowska and Sengers [30]. The data of Table 1 also confirm that our related common value $\gamma_c{}' = \left(\frac{p}{T}\right)_{\mathrm{CP}} + \pi_{\rho=\rho_c} T_c$ of the critical limiting slope of the critical isochore ($T > T_c$) and the saturation pressure curve ($T < T_c$) agrees with the values of Watanabe et al. [24], Biswas et al. [26], Biswas and Ten Seldam [27], Funke et al. [29], and Wyczalkowska and Sengers [30]. We note that the uncertainty $\left(^{+0.83\,\%}_{-1.20\,\%}\right)$ accounts for different values of the critical density, i.e., $\rho_c \simeq \rho = (734.3 \pm 0.2)\,\mathrm{kg}\cdot\mathrm{m}^{-3}$ ($T > T_c$) and $\rho_c = (742 \pm 4)\,\mathrm{kg}\cdot\mathrm{m}^{-3}$ ($T < T_c$) for Biswas et al. [26,27], $\rho_c = (742.26 \pm 0.40)\,\mathrm{kg}\cdot\mathrm{m}^{-3}$ ($T < T_c$) for Funke et al. [29], $\rho_c = (740 \pm 2)\,\mathrm{kg}\cdot\mathrm{m}^{-3}$ ($T < T_c$) for Watanabe et al. [24], and $\rho_c = (742 \pm \mathrm{n.a.})\,\mathrm{kg}\cdot\mathrm{m}^{-3}$ ($T < T_c$) for Wyczalkowska and Sengers [30]. Indeed, the

Table 2 Critical density value of SF_6 from recent experimental and modeling works

Author	Ref.	ρ_c ($kg \cdot m^{-3}$)	Precision	Method
DeBruijn	[31]	740.5 ± 0.3	0.04 %	Meniscus position
Funke et al.	[29]	742.26 ± 0.40	0.05 %	p, ρ, T measurements and non-linear fits
Wilkinson et al.	[9]	730 ± 7	1 %	*
Wyczalkowska and Sengers	[30]	$742 \pm$ n.a.	–	From Funcke et al.*
Haupt and Straub	[32]	$734.4 - 742.1$	1 %	*

* indicates a reference to a previous value for ρ_c found in literature

determination of ρ_c from density measurements in the two-phase domain ($T < T_c$) largely depends on the Ising value of the leading exponent in a non-linear fit of the coexisting liquid–gas density difference. To illustrate this literature status, some recent ρ_c determinations are reported in Table 2, including the latest one given by Funke et al. [29]. De Bruijn [31] reports an equivalent high level accuracy on the critical density value. However, De Bruijn's estimated value $\rho_c = (740.5 \pm 0.3)\,kg \cdot m^{-3}$ is not recovered by Funke et al.'s value. On their side, Haupt and Straub [32] correlate the values of T_c and ρ_c to the purity of the fluid sample in order to explain the different critical values obtained by the authors.

Since the Cassiopea mission, we have filled several similar sample cells at different densities bordering the critical density (in the ± 3 % range). Until now, the optical localization [12] of their liquid–gas meniscus close to the critical point have produced nine estimations of the critical density ranging from $738.2\,kg \cdot m^{-3}$ to $742.2\,kg \cdot m^{-3}$, with no asymptotic curvature of the rectilinear diameter (in the ± 0.1 % range). This result agrees with the values [9,29–32] reported in Table 2. The value $\rho_c = (740.2 \pm 2.0)\,kg \cdot m^{-3}$ was then used in the following analysis of the turbidity data.

The critical value n_c of the refractive index of SF_6 can be estimated from the Lorentz–Lorenz relation, with $\frac{M_{mole}}{\rho_c}\frac{n_c^2-1}{n_c^2+2} = 11.3906\,cm^3 \cdot mol^{-1}$ (see for example Ref. [33]). From $M_{mole} = 0.1460504\,g \cdot mol^{-1}$ and $\rho_c = 0.7402\,g \cdot cm^{-3}$, we have obtained $n_c = 1.0880$ for SF_6, with a precision of 1.2×10^{-4}. A laser stability of 0.3 % and a precision of 1.2×10^{-4} on n_c lead to an error bar of 0.35 % on the value of A. Then $\pi A = (101.51 \pm 0.35)\,J^{-1} \cdot m^{-4}$.

3.3 Crossover Behavior of ξ and κ_T

The crossover behaviors of the correlation length and the isothermal compressibility of SF_6 can now be calculated from the results of the massive renormalization scheme applied to the one-component fluids [34,8]. They are given by the following respective equations [35–37]

$$\left(\frac{1}{\alpha_c}\right)\xi\left(\Delta\tau^*\right) = \left(\mathbb{Z}_\xi^{\{1f\}}\right)^{-1}\ell_{th}(t_{th}) \tag{11}$$

$$(Z_c p_c)\,\kappa_T\left(\Delta\tau^*\right) = \left(\mathbb{Z}_\chi^{\{1f\}}\right)^{-1}\chi_{\rm th}(t_{\rm th}) \tag{12}$$

with

$$Y_c\Delta\tau^* = \left(\Theta^{\{1f\}}\right)^{-1} t_{\rm th} \tag{13}$$

In the right hand side of Eqs. 11, 12, and 13, $t_{\rm th}$ is the theoretical temperature-like field and $\Theta^{\{1f\}} = 4.288\times10^{-3}$, $\mathbb{Z}_\xi^{\{1f\}} = 25.6988$, $\mathbb{Z}_\chi^{\{1f\}} = 1950.70$ are three master (i.e., constant) numbers which are characteristics of the pure fluid subclass. The mean theoretical functions $[\ell_{\rm th}(t_{\rm th})]^{-1} = \mathbb{Z}_\xi^+(t_{\rm th})^\nu\prod_{i=1}^{N}\left(1+X_{{\rm i},\xi}^+(t_{\rm th})^{D(t_{\rm th})}\right)^{Y_{i,\xi}^+}$ and $[\chi_{\rm th}(t_{\rm th})]^{-1} = \mathbb{Z}_\chi^+(t_{\rm th})^\gamma\prod_{i=1}^{N}\left(1+X_{i,\chi}^+(t_{\rm th})^{D(t_{\rm th})}\right)^{Y_{i,\chi}}$ and the universal values [17] of the corresponding exponents and amplitudes of the $\{d=3, n=1\}$ universality class are defined in Refs. [34,8]. $D(t_{\rm th}) = \frac{\Delta_{\rm MF}S_2\sqrt{t_{\rm th}}+\Delta}{S_2\sqrt{t_{\rm th}}+1}$ is a universal mean crossover function for the confluent exponents $\Delta = 0.50189$ and $\Delta_{\rm MF} = \frac{1}{2}$ also defined in Ref. [8]. Therefore, the left-hand sides of Eqs. 11, 12, and 13 only introduce fluid-dependent parameters (α_c, p_c, Z_c, Y_c, etc.) which are defined from four critical coordinates, i.e., T_c, p_c, ρ_c, and $\gamma_c^{'}$, of the liquid–gas critical point of the selected one-component fluid [see Ref. [38] and [39]].[5] These four critical coordinates must be written as: $(\beta_c)^{-1} = k_{\rm B}T_c$ a energy unit, $\alpha_c = \left(\frac{k_{\rm B}T_c}{p_c}\right)^{\frac{1}{d}}$ a length unit, $Y_c = \gamma_c^{'}\frac{T_c}{p_c} - 1$ a scale factor of the dimensionless thermal field, and $Z_c = \frac{p_c m_{\bar{\rm p}}}{\rho_c k_{\rm B}T_c}$ a scale factor of the dimensionless ordering field ($m_{\bar{\rm p}}$ is the mass of the fluid particle). From the SF_6 critical parameters $T_c = 318.735\,{\rm K}$, $p_c = 3.754\,{\rm MPa}$, $\rho_c = 740.2\,{\rm kg\cdot m^{-3}}$, $\gamma_c^{'} = 0.0835\,{\rm MPa\cdot K^{-1}}$, and $m_{\bar{\rm p}} = 2.42522\times10^{-25}\,{\rm kg}$, we obtain: $(\beta_c)^{-1} = 4.40062\times10^{-21}\,{\rm J}$, $\alpha_c = 10.544\times10^{-10}\,{\rm m}$, $Y_c = 6.0896$, and $Z_c = 0.279501$.

In Fig. 4 are reported the residuals (expressed in %) for the literature data of ξ (part a) and κ_T (part b), from their estimation using Eqs. 11 and 12. The agreement with optical measurements performed far from the critical temperature is within 7 % with Cannell's [40] data for ξ and within 7 % with Feke et al.'s [41] data for κ_T. We note that these authors have also determined values for critical exponents ν and γ that differ from the ones selected in our estimation, increasing then the residuals for $T\to T_c$. Moreover, we note an excellent agreement to the leading power law obtained from interferometric measurements [42,43] (see the dashed green curves in Fig. 4b) or from thermodynamic property modeling [30] (see the mixed green curves in Fig. 4a, b). The upper axes of these Fig. 4a, b give the value of $\frac{\xi}{\alpha_c}$ that expresses the size of the density fluctuations in unit of the short range molecular interaction [35].

[5] see also condmat/0512408.

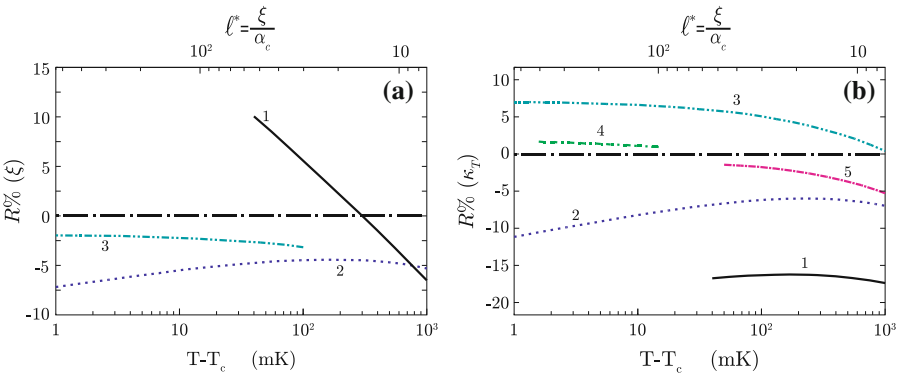

Fig. 4 Residuals (expressed in %) between published SF_6 data of ξ and κ_T and the calculated values using Eqs. 11 and (12), respectively. (**a**) The correlation length case: full (*black*) line labeled 1 [23]; tireted (*blue*) line labeled 2 [40]; double-dotted dashed (*cyan*) line labeled 3 [30]. (**b**) The isothermal compressibility case: full (*black*) line labeled 1 [23]; tireted (*blue*) line labeled 2 [40]; double-dotted dashed (*cyan*) line labeled 3 [30]; double-dashed dotted (*green*) line labeled 4 [42,43]; mixed (*pink*) line labeled 5 [41]

3.4 Asymptotic Singular Behavior of ξ and κ_T

For $\Delta\tau^* \to 0$, Eqs. 11 and 12 can be approximated by the following restricted Wegner-like expansions:

$$\xi = \alpha_c \xi^+ \left(\Delta\tau^*\right)^{-\nu} \left[1 + a_\xi^+ \left(\Delta\tau^*\right)^{\Delta} + \cdots\right] \tag{14}$$

$$\kappa_T = (p_c)^{-1} \Gamma^+ \left(\Delta\tau^*\right)^{-\gamma} \left[1 + a_\chi^+ \left(\Delta\tau^*\right)^{\Delta} + \cdots\right] \tag{15}$$

where the fluid-dependent amplitudes are given by $\xi_0^+ = \alpha_c \xi^+ = \alpha_c \left(Y_c\right)^{-\nu} \mathcal{Z}_\xi^+$, $\Gamma_0^+ \left(p_c\right)^{-1} \Gamma^+ = \left(p_c\right)^{-1} \left(Z_c\right)^{-1} \left(Y_c\right)^{-\gamma} \mathcal{Z}_\varkappa^+$, $a_\xi^+ = \left(Y_c\right)^{\Delta} \mathcal{Z}_\xi^{1,+}$, and $a_\chi^+ = \left(Y_c\right)^{\Delta} \mathcal{Z}_\varkappa^{1,+}$, respectively, (with $\frac{a_\xi^+}{a_\chi^+} = 0.68$). Here we use the master amplitude values $\mathcal{Z}_\xi^+ = 0.572902$, $\mathcal{Z}_\varkappa^+ = 0.11975$, $\mathcal{Z}_\xi^{1,+} = 0.37695$, and $\mathcal{Z}_\varkappa^{1,+} = 0.555$. These central values are based on the isothermal compressibility and coexisting liquid–gas density measurements near the critical point of xenon, which was then used as a standard Ising-like critical fluid described by the massive renormalization scheme (see Ref. [37]). Indeed for SF_6 we obtain: $\xi_0^+ = (1.926 \pm 0.014) \times 10^{-10}$ m (or $\xi^+ = 0.1826 \pm 0.0014$), $a_\xi^+ = 0.9334 \pm 0.0056$, $\Gamma_0^+ = (1.208 \pm 0.021) \times 10^{-8}\,\mathrm{Pa}^{-1}$ (or $\Gamma^+ = 0.0454 \pm 0.0008$), and $a_\chi^+ = 1.374 \pm 0.008$. The error bars account for uncertainties of ± 0.03 % on $\frac{p}{T}$ (i.e., ± 0.01 % on α_c), ± 0.3 % on ρ_c (i.e., ± 0.3 % on Z_c), and ± 1.2 % on $\gamma_c^{'}$ (i.e., ± 1.2 % on Y_c). The calculated values of the leading amplitudes ξ_0^+ and Γ^+ are in excellent agreement with the respective experimental results given in Refs. [3,40,42–44].

3.5 Fitting Results of Turbidity Data

Considering Fig. 3, τ_{expt} data can be compared to τ_{OZ} theoretical estimation using Eq. 8 with $\lambda_0 = 632.8\,\text{nm}$ (see the curve labeled τ_{OZ} in Fig. 3). In addition, Fig. 3 also presents other experimental data from [23] with corresponding theoretical estimation of τ_{OZ} accounting for $\lambda_0 = 466\,\text{nm}$.

Figure 3 indicates that the curve of Eq. 8 is in good agreement with our experimental data, except in the temperature range $T - T_c \lesssim 0.8\,\text{mK}$. The deviation is up to $\sim$33 % at $T - T_c \approx 50\,\mu\text{K}$ which corresponds likely to the closest temperature distance to T_c which was automatically reached on the ALICE 2 experiment on board the Mir station. Considering data from Puglielli and Ford [23], τ_{OZ} (right solid curve) is above the experimental points close to T_c, but in good agreement far from T_c, as shown in an inserted log–log scale presentation in Fig. 3. Note that the ξ values given on the upper axis of this insert can be directly used to estimate the value of $a = 2(k_0\xi)^2$, hence $F(a)$ of Eq. 9, approaching the critical point.

3.6 Deviation from Ornstein–Zernike Theory

The following analysis of the deviation between τ_{expt} and τ_{OZ} accounts for successively (i) the experimental errors on measured quantities involved in τ_{expt} of Eq. 1; (ii) the influence of the deviation of the sample to critical density; (iii) the influence of the multiple scattered light close to T_c; and (iv) the influence of the small finite value of the Green–Fisher η exponent which takes a zero value in τ_{OZ} of Eq. 8. The determination of ξ and κ_T are assumed "exact" along the critical isochore $\rho = \rho_c$ (see Sect. 3.4).

The uncertainty on B_τ is found to be the worst factor on the error level shown by the turbidity measurements at large distance of T_c (i.e., $T - T_c \gtrsim 500\,\text{mK}$, typically; see insert of Fig. 3). We conclude that the deviation with Eq. 8 near T_c cannot be explained by the actual measurement uncertainties.

As stated above, we have determined the deviation of our fluid sample to the critical density to be $\langle \delta\rho^* \rangle = (0.8 \pm 0.1)$ %, while $\rho_c = 740.2$ (± 0.27 %) $\text{kg}\cdot\text{m}^{-3}$ corresponds to our "mean" value of the critical density. The calculated temperature difference is $T_c - T_{\text{coex}} \approx 27\,\mu\text{K}$. Then it is probable that the precision on turbidity measurements very close to T_{coex}, i.e., $T - T_c \lesssim 300\,\mu\text{K}$, is mainly affected by the temperature uncertainty (of the order of 50 µK, as discussed above). On the other hand, the effect of the average off-critical density $\langle \delta\rho^* \rangle$ is more difficult to estimate in the absence of exact knowledge of the singular behavior of the correlation length when ρ is not exactly ρ_c. A practical approximation consists in connecting the correlation length to the susceptibility above the critical temperature, introducing the equation $\xi = \xi_0^+ \left(\frac{\kappa_T}{\Gamma_0^+}\right)^{\frac{\nu}{\gamma}}$ and neglecting the contribution of the confluent corrections. Using then the restricted cubic parametric model of the scaled equation of state [3] to estimate the respective effects of the off-critical density on the susceptibility, the correlation length and the turbidity, we have noted that our ratio $\frac{\tau_{\text{expt}}}{\tau_{\text{OZ}}(\rho=\rho_c)} \simeq 0.81$ at $T - T_c = 0.1\,\text{mK}$ corresponds to an estimated density difference

of $\rho - \rho_c \simeq 0.006\rho_c$. This value appears comparable to our measured off-criticality $\langle \delta\rho^* \rangle = (0.8 \pm 0.1)\,\%$. However, for $\rho - \rho_c \simeq 0.006\rho_c$, the corrected turbidity does not follow correctly the experimental behavior observed in the temperature range $0.6\,\mathrm{mK} \lesssim T - T_c \lesssim 3\,\mathrm{mK}$. Moreover, we recall that the above asymptotic equation that connects the correlation length to the isothermal compressibility is only strictly valid at $\rho = \rho_c$ when $\Delta\tau^* \to 0$. In addition, it is impossible to satisfy the Ising values for all asymptotic amplitude ratios in the cubic parametric model [45]. Therefore, we cannot conclude with certainty that the average off-critical density is the only parameter responsible for the deviation between τ_{expt} and τ_{OZ} approaching T_c. We also note that some other thermophysical property measurements performed close to T_c along the critical isochore, *de facto* refer to ρ_c values that roughly vary in the range $730\,\mathrm{Kg \cdot m^{-3}}$ to $742\,\mathrm{kg \cdot m^{-3}}$. The resulting data of the SF_6 properties "at critical density" can then be affected by the $\pm 0.82\,\%$ uncertainty around a lowered "central" value $\rho = 736\,\mathrm{kg \cdot m^{-3}}$ of the critical density (see Table 2). For example in their discussion on the validity of heat capacity measurement in SF_6, Haupt and Straub (HS) [32] consider being on the critical isochore within 1 %, using $\rho_c\,(\mathrm{HS}) = (737.2 \pm 0.27\,\%)\ \mathrm{kg \cdot m^{-3}}$ [i.e., $\langle \delta\rho^*_{HS} \rangle = (-0.4 \pm 0.3)\ \%$ from our critical density value], without any evaluation of a possible effect due to their average off-critical density.

In Fig. 2, we observe that the difference between experimental points and Eq. 8 occurs for $\tau \gtrsim 270\,\mathrm{m^{-1}}$. Considering Eq. 1, this value roughly corresponds to $R \lesssim \frac{1}{2}$. For $R \simeq \frac{1}{2}$ the scattered light at all angles starts to be of the same order as a transmitted light intensity and the possible contribution of a double, triple, etc., scattering mechanism cannot be ignored. Then, for the temperature range $T - T_c \lesssim 1\,\mathrm{mK}$, the contribution of the multiple light scattering cannot be neglected. This contribution can increase the I_2 value (on an amount that is difficult to estimate precisely), leading to a τ value lower than the one expected in Ornstein–Zernike theory, as observed experimentally (see Fig. 2).

We have investigated the influence of the Green–Fisher exponent η, previously taken equal to zero in Eq. 8, making then the Ornstein–Zernike formulation of the light scattering intensity not rigorously correct (see for example Refs. [46,47]). Here we have used the turbidity formulations given by Jacobs et al. [48]. For $\Delta\tau^* \leq 10^{-5}$, i.e., for $T - T_c \lesssim 3\,\mathrm{mK}$, τ reads as follows:

$$\tau = \frac{2\tau_0\,(\Delta\tau^*)^{-\gamma}}{a}\left[L - 1 - \frac{\eta}{4}L^2 + 8.37\eta\right] \tag{16}$$

where $L = \ln(2a)$ and $\tau_0 = \pi A T_c \Gamma_0^+$ in our previous notations. Value $\eta = 0.0336$ is taken from Ref. [17]. We note that $\eta = 0$ in Eq. 16 leads to the same result as the Ornstein–Zernike turbidity formulation of Eq. 8. However, we observe (see dotted curve on Fig. 3) that the maximum departure between both formulations [$\eta = 0$ or $\eta = 0.0336$ in Eq. 16] is less than 5 % at $T - T_c = 50\,\mu\mathrm{K}$. It is therefore not enough to explain the difference observed between our experimental points and the Ornstein–Zernike theory.

As a conclusive remark, we note that the deviation observed with our experimental points closer than 1 mK from T_c can only be accounted for by the off-critical density

of our cell and/or multiple scattering. Nevertheless, we believe that the approach of turbidity of SF_6 which follows Ornstein–Zernike theory through Eq. 8 incorporating ξ and κ_T values obtained from Eqs. 11 and 12, remains adequate for $T - T_c \gtrsim 3\,\mathrm{mK}$ range. On the other hand, anticipating the results of the next section, the "exact" values of ξ and κ_T, also appear in agreement with the Wilkinson et al.'s microgravity measurements of the asymptotic singular behavior of the thermal-diffusivity coefficient D_T close to T_c [9].

4 Asymptotic Singular Behavior of D_T

As proposed by Luettmer–Strathmann et al. [49], and validated by Wilkinson et al. [9] for the SF_6 case, the thermal diffusivity D_T can be written as an additive form $D_T = D_T^b + D_T^c$, where D_T^b is the background term and D_T^c is the critical term. Each contribution can then be expressed by a simple power law such that

$$D_T = D_0^b \left(\Delta\tau^*\right)^{\gamma} + D_0^c \left(\Delta\tau^*\right)^{\nu + x_\eta} \tag{17}$$

where γ, ν, and x_η are the universal exponents (see [17]). The fluid-dependent amplitudes D_0^b and D_0^c take the following convenient forms (see Ref. [9] for notations and definitions):

$$D_0^b = \left(\frac{T_c \lambda^b}{p_c}\right) \frac{1}{\Gamma^+} \left(\frac{T_c}{p_c}\frac{\partial p}{\partial T}\right)_{\rho_c}^{-2},$$

$$D_0^c = \frac{R_D k_B T_c \left(Q_0 \xi_0^+\right)^{-z_\eta}}{6\pi\,\eta_0 \xi_0^+}.$$

which can be calculated using our above estimations of the leading amplitudes $\Gamma^+ = \Gamma_0^+ p_c$ and ξ_0^+. The literature values are used for the other needed quantities (see Ref. [9]). Using the data reported in Table 3, we have obtained $D_0^b = 1.33 \times 10^{-6}\,\mathrm{m^2 \cdot s^{-1}}$ and $D_0^c = (3.97 \pm 0.24) \times 10^{-8}\,\mathrm{m^2 \cdot s^{-1}}$. Moreover, the relative deviations from the results given by Wilkinson et al. in Ref. [9] were well-defined through the following equations:

$$D_0^b = D_{0,W}^b \frac{T_c}{T_{c,W}} \frac{\Gamma_W^+}{\Gamma^+} = 1.004 D_{0,W}^b \tag{18}$$

$$D_0^c = D_{0,W}^c \frac{T_c}{T_{c,W}} \frac{\xi_{0,W}^+}{\xi_0^+} = 0.98 D_{0,W}^c \tag{19}$$

The subscript W refers to the Wilkinson et al.'s values (see Table 3 and related comment a), with $D_{0,W}^b = 1.32 \times 10^{-6}\,\mathrm{m^2 \cdot s^{-1}}$ and $D_{0,W}^c = (4.05 \pm 0.24) \times 10^{-8}\,\mathrm{m^2 \cdot s^{-1}}$.

To complement the Wilkinson et al.'s Fig. 6a of Ref. [9], $D_{T,\mathrm{expt}}$ data points from [9,19,41,50], and [31] are also reported in Fig. 5a. The related residuals $R\%\,(D_T) =$

Table 3 SF_6 property values for the determination of D_T

Property	Value	Reference
T_c	318.733 K	*
Γ_0^+	1.21×10^{-8} Pa^{-1}	*
ξ_0^+	1.92×10^{-10} m	*
p_c	3.76×10^6 Pa	[9]
$D^b_{0,W}$	1.32×10^{-6} m$^2 \cdot$ s^{-1}	[9] [a]
$D^c_{0,W}$	$(4.05 \pm 0.24) \times 10^{-8} \cdot$ m$^2 \cdot$ s^{-1}	[9]
$T_{c,W}$	318.769 K	[9]
Γ_W^+	0.046	[9,3]
$\xi^+_{0,W}$	$(1.88 \pm 0.06) \times 10^{-10}$ m	[9,44]

* Indicates a reference to this work

[a] R.A. Wilkinson, private communication, (2004). On the present work, we have used $\lambda^b = 0.035\,\mathrm{W \cdot m^{-1}\,K^{-1}}$ as a value of the background thermal conductivity for SF_6. Correspondingly, the amplitude value of the background term of the thermal diffusivity was $D^b_{0,w} = 1.32\,10^{-6}\,\mathrm{m^2 \cdot s^{-1}}$ [using the asymptotic form of Eq. (6.8) in Ref. [9] for the shear viscosity, where $\eta_0 = (3.99 \pm 0.04) \times 10^{-5}\,\mathrm{Pa \cdot s}$ and $\left(Q_0 \xi_0^+\right)^{-z_\eta} = 1.30 \pm 0.04$]

$100\left[\frac{D_{T,\mathrm{expt}}}{D_{T,\mathrm{calc}}} - 1\right]$ from $D_{T,\mathrm{calc}}$ of Eq. 17 are given in Fig. 5b. Our asymptotic formulation of Eq. 15 is close to the one of Wilkinson et al. [9], as shown in Fig. 5b by the residual deviations lower than 2.5 % between the (blue) full curve (Wilkinson case) and the (black) reference curve $R\%\,(D_T) = 0$ (our present case). We note that the full red curve in Fig. 5b corresponds to the residuals obtained using the complete crossover functions of ξ and κ_T [see Eqs. 11 and 12] and the complete background contributions of λ and η [19]. Although the background contribution seems a little overestimated, the interesting feature is that the critical term D_T^c fits well the experimental data close to T_c.

5 Conclusion

Using the microgravity conditions of the MIR space station, and the very good thermal environment of the ALICE 2 facility, we have obtained SF_6 turbidity data in a temperature range close to T_c. These data were analyzed using the Ornstein–Zernike theory introducing the calculated singular behavior of isothermal compressibility κ_T and correlation length ξ without adjustable parameters. A small deviation from the Ornstein–Zernike theoretical form for $T - T_c \lesssim 0.7$ mK can be partly attributed to multiple scattering and small critical density deviation. The estimated static and dynamic properties of SF_6 were successfully used to predict the asymptotic behavior of the thermal diffusivity, in agreement with the Wilkinson et al.'s microgravity measurements [9]. Such an accurate fluid description provides future confidence to

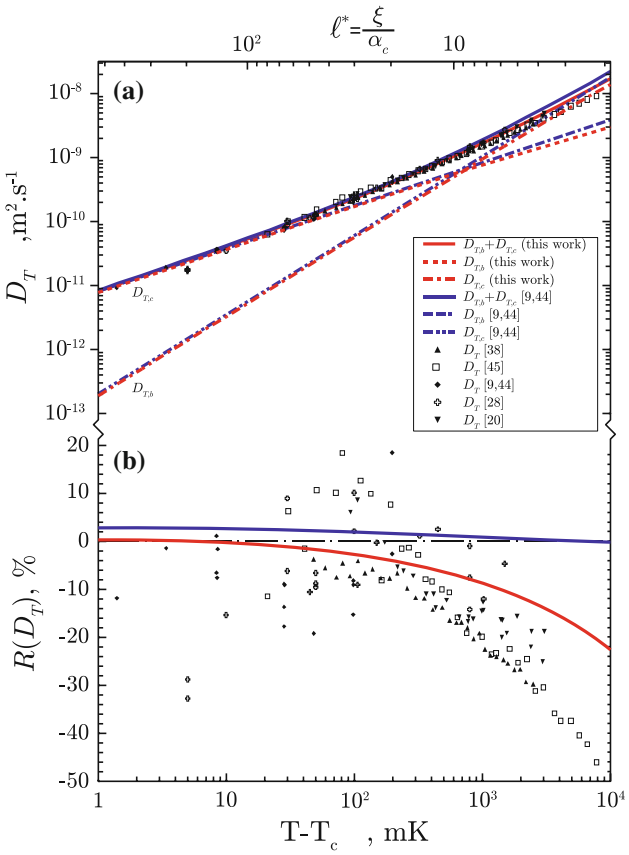

Fig. 5 (**a**) Thermal diffusivity as a function of $T - T_c$; solid (*red*) line: this work using Eqs. 17, 16, and 19; dotted (*black*) line: same equations from [9]; mixed (*blue*) line: background contribution D_T^b from [9]; dotted (*blue*) line: critical contribution D_T^c from [9]. Experimental data points are from [9,19,41,50], and [31] (see text); (**b**) corresponding residuals (%) from reference to our estimation (see text) using same lines and symbols as in **a** which also shows that the critical and background contributions are comparable at $T - T_c \approx 0.7\,\mathrm{K}$

manage SF_6 test cells very close to their liquid–gas critical point, in a space experiment [51] on board the International Space Station.

Acknowledgments ALICE (for Analyse des LIquides Critiques dans l'Espace) was a scientific program and ALICE 2 a facility, both supported by the French spatial agency CNES. We greatly acknowledge the French and Russian cosmonauts that made the experiment possible on board the Mir Space Station, and in particular the French spationaut Claudie Haigneré during the Cassiopea mission.

References

1. J. Zinn-Justin (ed.), *Euclidean Field Theory and Critical Phenomena*, 4th edn. (Clarendon, Oxford, 2002)

2. M.A. Anisimov, J.V. Sengers, in *Equations of State for Fluids and Fluid Mixtures*, part I, ed. by J.V. Sengers, R.F. Kayser, C.J. Peters, H.J. White, Jr. (Elsevier, Amsterdam, UK, 2000), pp. 381–434, and references therein
3. M.R. Moldover, J.V. Sengers, R. W. Gammon, R.J. Hocken, Rev. Mod. Phys. **51**, 79 (1979)
4. M. Barmatz, I. Hahn, J.A. Lipa, R.V. Duncan, Rev. Mod. Phys. **79**, 1 (2007)
5. R. Marcout, J.F. Zwilling, J.M. Laherrere, Y. Garrabos, D. Beysens, *ALICE 2, an advanced facility for the analysis of fluids close to their critical point in microgravity*, 45th Congress of the International Astronautical Federation, Jerusalem, Israel, 9–14 Oct 1994
6. L.S. Ornstein, F. Zernike, Proc. Acad. Sci. Amsterdam, **17**, 793 (1914)
7. L.S. Ornstein, F. Zernike, Phys. Z. **19**, 134 (1918)
8. Y. Garrabos, C. Bervillier, Phys. Rev. E **74**, 021113 (2006)
9. R.A. Wilkinson, G.A. Zimmerli, H. Hao, M.R. Moldover, R.F. Berg, W.L. Johnson, R.A. Ferrell, R.W. Gammon, Phys. Rev. E **57**, 436 (1998)
10. F. Perrot, D. Beysens, Y. Garrabos, T. Fröhlich, P. Guenoun, M. Bonetti, P. Bravais, Phys. Rev. E **59**, 3079 (1999)
11. Y. Garrabos, A. Dejoan, C. Lecoutre, D. Beysens, V. Nikolayev, R. Wunenburger, J. Phys. IV **11**, 6–23 (2001)
12. C. Morteau, M. Salzmann, Y. Garrabos, D. Beysens, in *Proceedings of the Second European Symposium "Fluids in Space"*, ed. by A. Viviani, Neaple, Italy, 22–26 April 1996 (Edizioni Jean Gilder Congressi srl, Neaple), pp. 327–333
13. D. Beysens, Y. Garrabos, V.S. Nikolayev, C. Lecoutre-Chabot, J.P. Delville, J. Hegseth, Europhys. Lett. **59**, 245 (2002)
14. Y. Garrabos, M. Bonetti, D. Beysens, F. Perrot, T. Frölich, P. Carlès, B. Zappoli, Phys. Rev. E **57**, 5665 (1998), and references therein
15. P. Guenoun, D. Beysens, Y. Garrabos, F. Kammoun, B. Le Neindre, B. Zappoli, Phys. Rev. E **47**, 1531 (1993)
16. V.S. Nikolayev, A. Dejoan, Y. Garrabos, D. Beysens, Phys. Rev. E **67**, 061202 (2003)
17. R. Guida, J. Zinn-Justin, J. Phys. A : Math. Gen. **31**, 8103 (1998)
18. H. Hao, R.A. Ferrell, J.K. Bhattacharjee, Phys. Rev. E **71**, 021201 (2005)
19. A. Letaief, R. Tufeu, Y. Garrabos, B. Le Neindre, J. Chem. Phys. **84**, 921 (1986)
20. J. Straub, K. Nitsche, Fluid Phase Equilib. **88**, 183 (1993)
21. J. Straub, A. Haupt, L. Eicher, Int. J. Thermophys. **16**, 1033 (1995)
22. R.A. Ferrell, H. Hao, Physica A **197**, 23 (1993)
23. V.G. Puglielli, N.C. Ford, Phys. Rev. Lett. **25**, 143 (1970)
24. K. Watanabe, H. Watanabe, K. Oguchi, in *Proceedings of the seventh Symposium on Thermophysical properties*, ed. by A. Cezairliyan (ASME, New York, 1977), p. 489
25. K.M. de Reuck, R.J.B. Craven, W.A. Cole, *Report on the development of equation of state for sulfur hexafluoride*, IUPAC Thermodynamic Tables Project Centre : London (1991)
26. S.N. Biswas, N.J. Trappeniers, J.H.B. Hoogland, Physica A **126**, 384 (1984)
27. S.N. Biswas, C.A. Ten Seldam, Fluid Phase Equilib. **47**, 67 (1989)
28. W. Wagner, N. Kurzeja, B. Pieperbeck, Fluid Phase Equilib. **79**, 151 (1992)
29. M. Funke, R. Kleinrahm, W. Wagner, J. Chem. Thermodyn. **34**, 735–754 (2002)
30. A. Kostrowicka Wyczalkowska, J.V. Sengers, J. Chem. Phys. **111**, 1551 (1999)
31. R. DeBruijn, Doctoral Dissertation, ISBN 90-5776-021-5 (1999)
32. A. Haupt, J. Straub, Phys. Rev. E, **59**, 1795 (1999)
33. J. Obriot, J. Ge, T.K. Bose, J.-M. St. Arnaud, Fluid Phase Equilib. **86**, 315–350 (1993)
34. C. Bagnuls, C. Bervillier, Phys. Rev. E **65**, 066132 (2002)
35. Y. Garrabos, C. Lecoutre, F. Palencia, C. Erkey, B. LeNeindre, Phys. Rev. E **73**, 026125 (2006)
36. Y. Garrabos, Phys. Rev. E **73**, 056110 (2006)
37. Y. Garrabos, C. Lecoutre, F. Palencia, B. LeNeindre, C. Erkey, Phys. Rev. E **77**, 021116 (2008)
38. Y. Garrabos, J. Phys. (Paris) **46**, 281 (1985)
39. Y. Garrabos, J. Phys. (Paris) **47**, 197 (1986)
40. D.S. Cannell, Phys. Rev. A **21**, 225 (1975)
41. G.T. Feke, G.A. Hawkins, J.B. Lastovka, G.B. Benedek, Phys. Rev. Lett. **27**, 1780 (1971)
42. R. Hocken, M.R. Moldover, Phys. Rev. Lett. **37**, 29 (1976)
43. J.V. Sengers, M.R. Moldover, Phys. Lett. **66A**, 44 (1978)
44. M.R. Moldover, Phys. Rev. A **31**, 1022 (1985)

45. M.E. Fisher, S.-Y. Zinn, P.J. Hupton, Phys. Rev. B **59**, 14533 (1999)
46. M.E. Fisher, J. Math. Phys. **5**, 944 (1964)
47. R.A. Ferrell, Phys. A **177**, 201–206 (1991)
48. D.T. Jacobs, S.M. Lau, A. Mukherjee, C.A. Williams, Int. J. Thermophys. **20**, 877 (1999)
49. J. Luettmer-Strathmann, J.V. Sengers, G.A. Olchowy, J. Chem. Phys **103**, 7482 (1995)
50. P. Jany, J. Straub, Int. J. Thermophys. **8**, 165 (1987)
51. R. Marcout et al, 57th Congress of the International Astronautical Federation, Valencia, Spain, 2–6 Oct (2006), paper IAC-06-A2.5.02